Analytical calculation of stopping power for isolated small spheres

T. L. Ferrell, R. J. Warmack, and V. E. Anderson
Health and Safety Research Division, Oak Ridge National Laboratory, Oak Ridge, Tennessee 37831

P. M. Echenique
Cavendish Laboratory, Cambridge CB3 0HE, England
and Euskal Herriko Unibertsitatea, Quimicas, Donostia, Euskadi, Spain
(Received 25 September 1986)

A charged particle passing near a spherical body engenders real collective excitations which contribute to the stopping power. The greatest contributions occur at small impact parameters where many multipoles are excited on the spherical surface. An analytical form for these contributions is obtained for spheres that are sufficiently small that retardation is negligible and which are characterized by a spatially local, frequency-dependent dielectric function. Results are given for a variety of materials for which the optical-uv properties are known.

I. INTRODUCTION

This paper presents calculations of energy-loss rates to collective excitations for charged particles interacting with a sphere. The sphere is characterized by a spatially local, frequency-dependent dielectric function $\epsilon(\omega)$, and is assumed to be sufficiently small that retardation is negligible. This problem is of general interest, but our work is motivated by considerations of energy losses by low-energy electron beams in aloof scattering near a surface,[1] and by similar considerations related to scanning transmission electron microscopy,[2–4] as indicated in an earlier letter.[5] However, a detailed comparison with the great variety of relevant experimental data is beyond the scope of this paper and we simply show general results for several types of targets. Since the results obtained are relatively straightforward to apply to any given beam profile, we do not attempt to specialize the calculation to any single profile. Our main concern is that the strongest surface effects occur for passage of the beam close to the target where high orders of multipolar excitations occur, these modes being rather complicated to analyze in previous treatments.[6–8] By obtaining a simple analytical calculation of such effects, we are able to give a succinct result valid for all impact parameters and which may be applied to any material with known optical properties.

In Sec. II we consider a charged particle moving at constant velocity outside a small sphere and find the work done in order to maintain the constant velocity. This expression in turn yields the differential energy-loss probability. In quantum terms, the charge excites both real and virtual collective effects, the former giving rise to energy dissipation and the latter to conservative effects. Both effects can be encoded in a complex self-energy function, and possible excitations include surface plasmons,[8–10] surface optical phonons,[11] helicons, ripplons,[12] and quanta of orientation effects on permanent molecular dipoles.[13] The classical analysis is in agreement with the quantum results in all these cases as long as the frequency is converted to energy by multiplication of Planck's constant in the final result. We present the details of this analysis for the charge in one medium and the sphere composed of a material of different dielectric function, a result of particular interest in producing chemical maps of composite materials by electron energy-loss analysis.

In Sec. III we consider the sphere to be surrounded by a layer of material different from that of the sphere or of the surrounding material. This case is of importance for materials which readily form a thin oxide or sulfide layer on their surfaces. The result obtained has the same dependence upon impact parameter as the case without a layer and thus can be numerically evaluated with equal facility.

In Sec. IV, we consider a range of several distinctly different materials, including metals, semiconductors, and organic compounds for which optical constants are available. In each case we give the differential probability of a given incremental energy loss as a function of the loss, presenting the results for several incident beam energies at near grazing incidence. We present our conclusions about these results in Sec. V.

II. ALOOF SCATTERING NEAR A SPHERE

Consider a point charge q moved at constant velocity $\mathbf{v}$ along a trajectory specified in Cartesian coordinates by $z'=vt$, $x'=b$, $y'=0$, at time t, and with $v \ll c$. In terms of spherical coordinates (r,θ,ϕ), one has r' equal to $(b^2+z'^2)^{1/2}$ and $\cos\theta'$ equal to z'/r'. The scalar electric potential at (r,θ,ϕ) for $r'>r$ is

$$\frac{q}{|\mathbf{r}-\mathbf{r}'(t)|}=\frac{q}{r'}\sum_{l=0}^{\infty}\sum_{m=0}^{l}N_{lm}\left[\frac{r}{r'}\right]^{l}P_{lm}(\cos\theta)\times P_{lm}(\cos\theta')\cos(m\phi)\,, \quad (1)$$

where P_{lm} is the associated Legendre function as given by Stratton.[14] Also,

$$N_{lm}=\frac{(2-\delta_{0m})(l-m)!}{(l+m)!}\ , \tag{2}$$

where δ_{0m} is unity for $m=0$ and is zero otherwise. If $r>r'$, then r and r' are exchanged in Eq. (1).

If one uses spatially local, frequency-dependent, complex, dielectric functions to characterize the electrodynamic response of the (nonmagnetic) media involved, it is necessary to introduce Fourier transforms to match boundary conditions. That is, for any time-dependent function $f(t)$, one writes

$$\tilde{f}(\omega)=\int_{-\infty}^{\infty}f(t)e^{i\omega t}dt \tag{3}$$

assuming the integral exists, and

$$f(t)=\int_{-\infty}^{\infty}\tilde{f}(\omega)e^{i\omega t}\frac{d\omega}{2\pi}\ . \tag{4}$$

We now consider a sphere of radius $a<b$ centered at the origin and having dielectric function $\epsilon(\omega)=\epsilon_1(\omega)+i\epsilon_2(\omega)$, where ϵ_1 is the real part of ϵ and ϵ_2 is its imaginary part. The charge is assumed to move in a medium of dielectric function $\bar{\epsilon}(\omega)=\bar{\epsilon}_1(\omega)+i\bar{\epsilon}_2(\omega)$.

If $\tilde{\Phi}_q$ is the Fourier transform of the potential Φ_q due to q as given in Eq. (1) for $r'>r$, then the potential outside the sphere has Fourier transform

$$\tilde{\Phi}_{\rm out}=\frac{\tilde{\Phi}_q}{\bar{\epsilon}(\omega)}+\sum_{l=0}^{\infty}\sum_{m=0}^{l}A_{lm}(2-\delta_{0m})\left[\frac{a}{r}\right]^{l+1}\times P_{lm}(\cos\theta)\cos(m\phi) \tag{5}$$

and inside the sphere the Fourier component of the potential is

$$\tilde{\Phi}_{\rm in}=\sum_{l=0}^{\infty}\sum_{m=0}^{l}B_{lm}(2-\delta_{0m})\left[\frac{r}{a}\right]^{l}P_{lm}(\cos\theta)\cos(m\phi)\ , \tag{6}$$

where terms odd in the angle ϕ are omitted as they are inconsequential. The Fourier transform of Φ_q requires the integral

$$I_{lm}=\int_{-\infty}^{\infty}r'^{-(l+1)}P_{lm}(\cos\theta')e^{i\omega z'/v}d(z'/v)\ . \tag{7}$$

To perform this integration we took the tedious route of calculating it for several values of the indices, observing a pattern in the results, and then proving the inferred answer by induction. We have since obtained more elegant and simpler proofs, and note that it is given in the literature[15] in terms of Meijer's function (a rather inconvenient answer). Of course, once the integral is known, mathematical induction is a straightforward manner of proof. We find

$$I_{lm}=\frac{2i^{l-m}|k|^{l}K_m(|kb|)}{v(l-m)!}\left[\frac{k}{|k|}\right]^{l-m}\ , \tag{8}$$

where $k=\omega/v$, and K_m is the modified Bessel function of order m.

Matching the potentials (5) and (6) at $r=a$ and similarly matching their normal derivatives multiplied by the dielectric function appropriate to each, one obtains two equations which may be solved for A_{lm}. This gives the homogeneous portion of the external potential $\tilde{\Phi}_0$ in frequency space. One finds that the $l=0$ term identically vanishes, leaving

$$\tilde{\Phi}_0=-q\sum_{l=1}^{\infty}\sum_{m=0}^{l}N_{lm}a^{l-3}[a_l(\omega)+\beta_l(\omega)+\gamma(\omega)]\times\left[\frac{a}{r}\right]^{l+1}f_{lm}I_{lm}\ , \tag{9}$$

where f_{lm} stands for $P_{lm}(\cos\theta)\cos(m\phi)$, the integral I_{lm} is given by (7), while N_{lm} is given by (2), and $a^{-3}\gamma(\omega)$ stands for $-1+[1/\bar{\epsilon}(\omega)]$, the reduction in the volume-plasmon contribution due to the presence of the surface (the so-called *begrenzung* term[16] which is neglected henceforth, as discussed below), and

$$\beta_l(\omega)=\frac{a^3(2l+1)[\bar{\epsilon}(\omega)-1]}{[l\epsilon(\omega)+\bar{\epsilon}(\omega)(l+1)]} \tag{10a}$$

while

$$a_l(\omega)=a^3\left[\frac{\epsilon(\omega)-\bar{\epsilon}(\omega)}{\epsilon(\omega)+[(l+1)\bar{\epsilon}(\omega)/l]}\right] \tag{10b}$$

is the l-dependent polarizability. Although we neglect the *begrenzung* term and volume losses, the surface losses occur at energies well separated from the energy of the volume plasmon. Even in silver (for which the volume plasmon has an energy of 3.72 eV) the energy loss for the highest-order modes is 0.1 eV less than the volume-plasmon energy, and silver has one of the smallest differences in energy between the bulk and surface plasmons. Defining

$$\frac{dW}{dz}=q\left.\frac{\partial\Phi_0}{\partial z}\right|_{r'=r} \tag{11}$$

one has also by letting $\bar{\alpha}_l(\omega)$ replace $\alpha_l(\omega)+\beta_l(\omega)$ that

$$\frac{dW}{dz}=q^2\sum_{l,m}\int_{-\infty}^{\infty}\frac{dw}{2\pi}e^{-i\omega z/v}\bar{\alpha}_l(\omega)\frac{a^{2l-2}}{r^{l+2}}(l+1-m)\times N_{lm}I_{lm}P_{l+1,m}(\cos\theta)\ , \tag{12}$$

where the coordinates referring to the location of q are now left unprimed.

If one converts (12) to positive limits on ω after integrating z from negative to positive infinity, then the work done in maintaining constant velocity is found to be

$$W=\frac{8q^2}{va^3}\sum_{l,m}M_{lm}\int_0^{\infty}\frac{dw}{2\pi}K_m^2(\omega b/v)(\omega a/v)^{2l+1}{\rm Im}\bar{\alpha}_l(\omega)\ , \tag{13}$$

where ${\rm Im}\bar{\alpha}_l(\omega)$ is the imaginary part of the generalized polarizability and

$$M_{lm}=\frac{(2-\delta_{0m})}{(l-m)!(l+m)!}\ . \tag{14}$$

The differential energy-loss probability is defined in Hartree atomic units ($e=m=\hbar=1$) by

$$W=\int_0^\infty d\omega\,\omega\frac{dP}{d\omega} \tag{15}$$

so that for an electron the differential probability is

$$\frac{dP}{d\omega}=\frac{4a^{-2}}{\pi v^2}\sum_{l,m}M_{lm}\left[\frac{\omega a}{v}\right]^{2l}K_m^2\left[\frac{\omega b}{v}\right]\mathrm{Im}\bar{\alpha}_l(\omega)\ . \tag{16}$$

For each value of l and m the critical value of the differential energy-loss probability as a function of v occurs at $v=v_1$, the first derivative with respect to v vanishing for each mode at $v=v_1$ to give

$$(l+1+m)K_m\left[\frac{\omega b}{v_1}\right]=\left[\frac{\omega b}{v_1}\right]K_{m+1}\left[\frac{\omega b}{v_1}\right]\ . \tag{17}$$

The second derivative at this value of v is

$$S_{lm}=2K_m^2(\omega b/v_1)v_1^{-2(l+2)}\left[\left[\frac{\omega b}{v_1}\right]^2-(l+1)^2+m^2\right]\ . \tag{18}$$

If $\omega b/v_1$ is large compared to unity, then the Bessel functions lie in the asymptotic regime and Eq. (17) demands $l+1+m$ be large. Then S_{lm} is positive and v_1 gives a minimum value to the large-order contribution. No value of v_1 satisfies Eq. (17) for $\omega b/v_1\ll 1$. For low order, $\omega b/v_1$ is on the order of unity and one has a *maximum* in the low-order contribution at $v=v_1$. In the dipole case $l=1,m=0$, one has $\omega b/v_1$ from Eq. (17) must be about 1.65 and $S_{10}<0$. Then for a silver sphere with ω evaluated at the dipolar surface plasmon energy ($\omega\sim 0.13$) and $b=200$ bohr radii, one finds the energy $E_1=v_1^2/2$ to be about 124 Hartree rydbergs (1 Hartree rydberg = 27.2 eV), or roughly 3.4 keV. Above this energy the $m=0$ dipole contribution drops with increasing beam energy. For materials with a higher surface-plasmon energy the maximum occurs at higher energies, e.g., for aluminum, the maximum occurs at an incident electron energy of about 39.2 keV.

Equation (16) can be applied to several cases. If one has a vacuum outside a condensed matter sphere, then $\bar{\epsilon}=1$ and $\epsilon(\omega)$ can be obtained from the bulk optical properties of the material of the sphere so long as the sphere contains a sufficient number of atoms. For spheres on the order of several nanometers in size many hundreds or even thousands of atoms are present and it can be expected that bulk optical properties are sufficient. Application of the results in this instance to several materials is given in Sec. IV. If one considers the case of a spherical void, then $\epsilon=1$ and $\bar{\epsilon}(\omega)$ is the dielectric function of the medium containing the void. Both cases are of interest in transmission of electron beams through samples and near microspheres. For materials present both inside and outside the sphere two different files of optical data must be called in applying the calculations, but the simplicity of Eq. (16) allows this to be done with an economical program. The more severe problem comes for near-grazing incidence, a case requiring up to a hundred values of l. This necessitates a program for calculating high-order Bessel functions accurately, and for dealing with underflows. By use of downward recurring formulas the Bessel functions can be accurately tabulated, and by judicious use of logarithms the underflows can be eliminated. Otherwise the calculations proceed in a straightforward way.

III. THE SPHERE WITH A LAYER

It is not uncommon to find that a small sphere oxidizes or in some other fashion obtains a thin layer on its surface with very different optical properties from those of the interior. Indeed, for aluminum, the oxide layer is very difficult to avoid even under ultrahigh vacuum for a time sufficient to complete an experiment. In this section, we consider the effects of a layer on the differential energy loss probability per incremental energy loss. Schmeits has given an analysis of the dipole limit in this case.[17]

Let a sphere of radius a_1 be surrounded by a concentric layer between $r=a_1$ and $r=a_2$, the dielectric function of the interior being $\epsilon(\omega)$ and that of the layer being $\hat{\epsilon}(\omega)$. The dielectric function of the material outside the layer ($r>a_2$) is denoted $\bar{\epsilon}(\omega)$. Due to coupling, the layer sustains two surface-plasmon energies for each mode of a bare sphere. Thus, the dispersion relationship

$$\epsilon(\omega)=-(l+1)\bar{\epsilon}(\omega)/l \tag{19}$$

for a bare sphere becomes a quadratic relationship involving $\hat{\epsilon}(\omega)$ when a layer is present. We find from elementary electrodynamics that

$$0=\hat{\epsilon}^2(\omega)+\frac{\hat{\epsilon}(\omega)}{1-g_l}\left[\bar{\epsilon}(\omega)\left[\frac{l+1}{l}+g_l\right]+\epsilon(\omega)\left[\frac{l}{l+1}+g_l\right]\right]$$
$$+\epsilon(\omega)\bar{\epsilon}(\omega)\ , \tag{20}$$

where g_l is $(a_1/a_2)^{2l+1}$ which is assumed not to be unity here. If $a_1=a_2$, then the term in square brackets vanishes because Eq. (19) holds. Since all the dielectric functions involved are complex, in general Eq. (20) is never satisfied for real frequencies, as is the usual case with surface-plasmon dispersion relations. But in energy-loss problems, Eq. (20) occurs in the denominator of the imaginary part of the energy-loss function and merely gives rise to finite-width peaks in this function at the surface plasmon frequencies.

The scalar electric potential has a Fourier frequency component for $r>a_2$ which is denoted as $\tilde{\Phi}_{\mathrm{out}}$ and is given by Eq. (5) but with $a=1$ for purposes of convenience here. For $a_1<r<a_2$ the potential has frequency component

$$\tilde{\Phi}_{\mathrm{bet}}=\sum_{l,m}\frac{C_{lm}}{g_l-1}f_l(2-\delta_{0m})P_{lm}(\cos\theta)\cos(m\phi) \tag{21}$$

with the subscript "bet" meaning "between" a_1 and a_2, while

$$f_l=\frac{g_l(B_l-1)r^l}{a_1^{2l+1}}+\frac{g_l-B_l}{r^{l+1}} \tag{22}$$

and B_l is an amplitude to be determined. Also, for $r<a_1$ one has

$$\tilde{\Phi}_{\rm in}=\sum_{l,m} C_{lm}B_l(2-\delta_{0m})\frac{r^l}{a_1^{2l+1}}P_{lm}(\cos\theta)\cos(m\phi)\ . \quad (23)$$

In order that the potential be continuous

$$C_{lm}=A_{lm}+q\frac{(l-m)!a_2^{2l+1}}{(l+m)!\bar{\epsilon}(\omega)}I_{lm}\ . \quad (24)$$

Applying the continuity of the normal components of the electric displacement vector in frequency space one finds

$$A_{lm}=-\frac{qa_2^{2l+1}I_{lm}(l-m)!}{\bar{\epsilon}(\omega)(l+m)!}(1+D_{lm})\ , \quad (25)$$

where

$$D_{lm}=\frac{(2l+1)[\epsilon(\omega)(1-g_l)-\hat{\epsilon}(\omega)(lg_l+l+1)]}{l(l+1)[\hat{\epsilon}(\omega)-\epsilon_+][\hat{\epsilon}(\omega)-\epsilon_-](1-g_l)} \quad (26)$$

with ϵ_+ and ϵ_- being the two values of $\hat{\epsilon}(\omega)$ given by the two roots of Eq. (20). The amplitude A_{lm} contains the *begrenzung* term which may be omitted by retaining only D_{lm} in the parenthesis in Eq. (25). The modified coefficient A_{lm} then contains only the surface plasmon effects for $l\geq 1$ and may be separated into two coefficients using partial fractions if desired.

We find for the surface plasmon contribution to the differential probability of losing energy between ω and $\omega+d\omega$ (in Hartree atomic units)

$$\frac{dP}{d\omega}=\frac{4a_2^{-2}}{\pi v^2}\sum_{l,m}M_{lm}\left[\frac{\omega a_2}{v}\right]^{2l}K_m^2\left[\left|\frac{\omega b}{v}\right|\right]\frac{(2l+1)}{l(l+1)}{\rm Im}\zeta_l\ , \quad (27)$$

where

$$\zeta_l=\frac{a_2^3}{1-g_l}\left[\frac{\epsilon(\omega)l(1-g_l)-\hat{\epsilon}(\omega)(lg_l+l+1)}{[\hat{\epsilon}(\omega)-\epsilon_+][\hat{\epsilon}(\omega)-\epsilon_-]}\right]\ . \quad (28)$$

For $a_1\to a_2$ and $\hat{\epsilon}\to\epsilon$, Eq. (27) yields Eq. (16). Since the same sum on the azimuthal index m occurs in Eq. (27) as in Eq. (16), one may calculate the effect of the layer by comparing the dependences on the mode index. We consider only the unlayered sphere for presentation of the results in the next section, as the numerous possible combinations of materials for display of Eq. (27) would require a rather lengthy exposition. Indeed, once an algorithm is developed for Eq. (16), it is not difficult to modify it to selected cases appropriate to individual experiments.

IV. ANALYSIS OF SPECIFIC CASES

To illustrate the application of Eq. (16) to a variety of cases without embarking upon a complex trail of the many combinations of materials which may be of interest, we first take $\bar{\epsilon}(\omega)=1$. This is the case of a vacuum-bounded sphere. We then consider several materials, including metals, semiconductors, and insulators. Figure 1 shows our results for an aluminum sphere bounded by vacuum. A graph of $\log_{10}(dP/dE)$, for $E=\hbar\omega$ in Hartree atomic units ($e=\hbar=m=1$) versus ω (or E) is shown for a sphere of radius 10 nm and for $b=10.4$ nm. Several different curves are displayed, each corresponding to a given energy of the incident beam of electrons. All of the ensuing cases assume the same spherical radius, impact parameter, and incident energies. Figure 2 shows the results for a silver sphere bounded by vacuum, and Fig. 3 gives the same results for gold. The beam energies for each curve in each of the figures are 100 eV, 500 eV, 2.5 keV, 10 keV, and 50 keV. The results at 100 eV are always shown as a dashed curve, while the other energies are distinguished by the fact that the excitation probability at the central peak diminishes with increasing beam energy above 100 eV. In all cases presented, the sum on l gave sufficient accuracy by including 100 values of l. We used a Digital Equipment Corporation PDP/1123 microcomputer, all programs being written in FORTRAN. Run times were on the order of 5 min.

In the case of aluminum, there is a double peak for a 50-keV beam, the splitting being due to the separation of the dipole from the higher modes. Higher values of the incident energy are not perfectly equivalent to smaller impact parameters, of course, but the argument of the Bessel function is $\omega b/v$. As a consequence of this dependence there are higher mode excitations at higher energies. Also, note that for aluminum the 100-eV curve has a lower peak height at its maximum than does the 500-eV

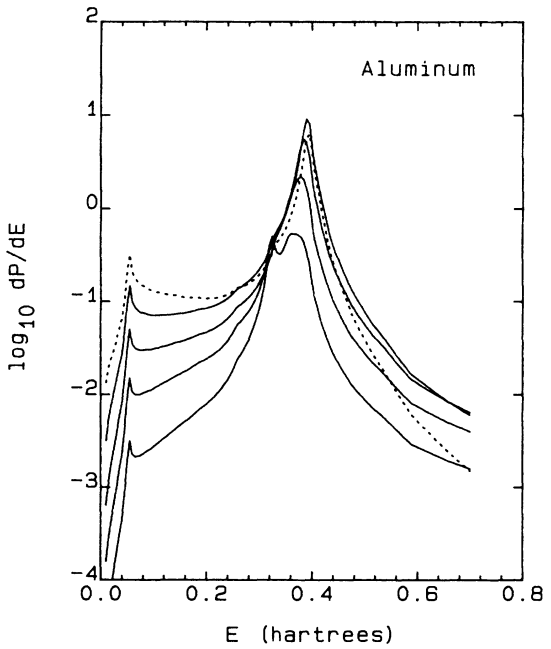

FIG. 1. The logarithm to base ten of the differential energy loss probability dP/dE vs the energy loss E in Hartree atomic units for an electron passing at a distance of 208 bohr radii from the center of a vacuum-bounded aluminum sphere of radius 200 bohr radii. The dotted curve is for a 100-eV incident beam, while the remaining curves in descending peak height for increasing beam energies are for 500 eV, 2.5 keV, 10 keV, and 50 keV.

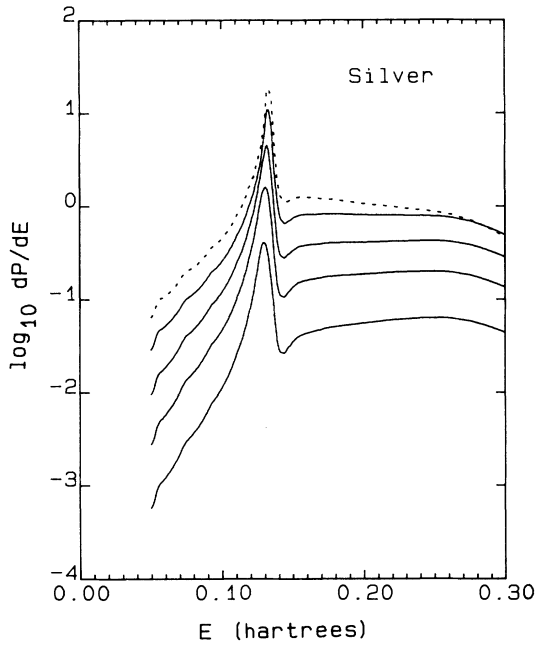

FIG. 2. Same as Fig. 1, except that the sphere is made of silver.

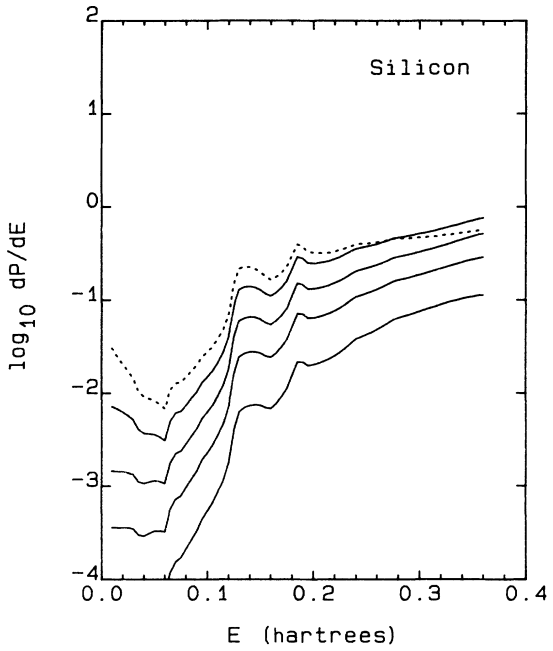

FIG. 4. Same as Fig. 1, except that the sphere is made of silicon.

curve. The same does not hold for silver and gold due to their relatively lower surface-plasmon energies. Additional details of the mode dependence are given in the paper by Ferrell and Echenique.[5]

In Fig. 4 we show the results for a vacuum-bounded silicon sphere. Due to the extraordinary variations in the dielectric function of silicon, the results increase as a function of ω with the surface-plasmon peaks being mere bumps on the way to ever-larger loss probabilities. As in the case of metals the 100-eV curve drops below the other curves for the region of ω above the point where the curve has its peak. For polystyrene, which is used in the results

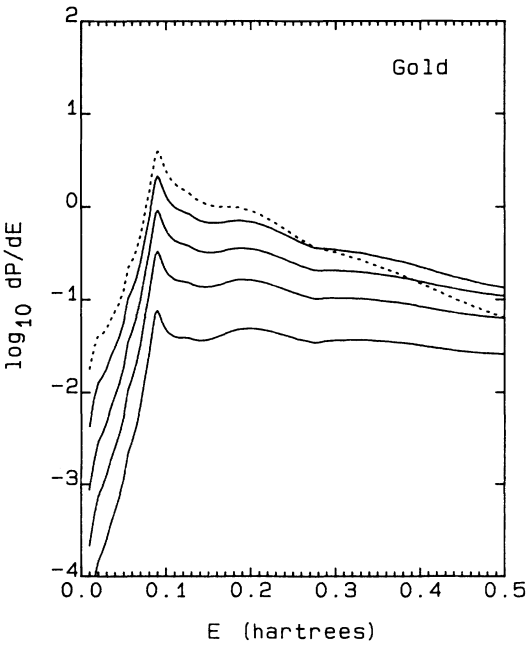

FIG. 3. Same as Fig. 1, except that the sphere is made of gold.

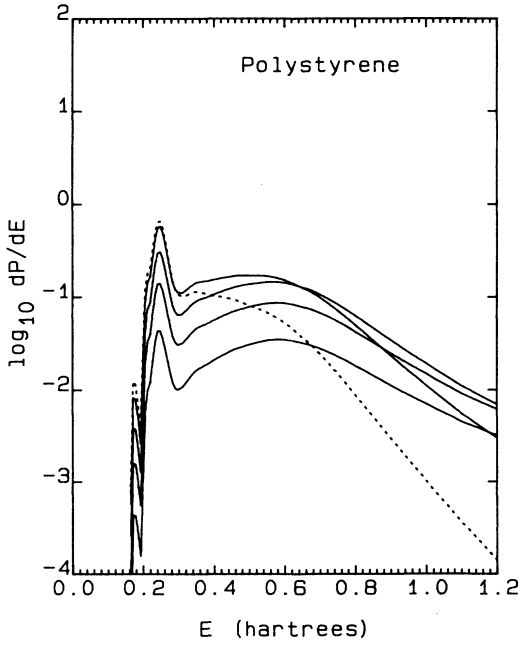

FIG. 5. Same as Fig. 1, except that the sphere is made of polystyrene.

for Fig. 5, the 500-eV curve also drops below the higher-energy curves in the region of the higher values of ω. Despite the larger values of $\epsilon_2(\omega)$ for silicon and polystyrene relative to the metals, there is a definite energy-loss peak. In order to demonstrate that possible applications may be obtained for biological systems we show results for water in Fig. 6 and for adenine in Fig. 7. In practical situations one should include a surrounding dielectric in these cases, but we present the vacuum-bounded case partly to show the case of applicability of the results to any material with known optical properties.[18]

In Fig. 8 we show the effect of a surrounding material by considering an aluminum sphere surrounded by manganese. For this figure only the solid curve is for 100-eV beam, while the other curves diminish at the peak for ever-higher energies, the same set of energies being used as for the other figures. The effect of the manganese substantially alters the results over the case of Fig. 1. A broad peak appears near the volume-plasmon energy of aluminum, this blue shift from the usual aluminum surface plasmon being due to the rather complicated combination of the two complex dielectric functions. We have presented dP/dE rather than its logarithm as the variation in amplitude is not nearly so extreme as in the vacuum bounded case for the various curves.

We have not attempted to average over impact parameters; since this procedure depends in detail upon the beam profile, it must be left to individual experiments. The major influence of such profiles might for instance be the enhancement of the dipole mode contribution for aloof scattering, as there are ever more particles in the beam as one moves outward from the surface of the sphere. The particles with larger impact parameter, being more numerous and tending to excite the dipole mode most strongly, could cause such a result, but one must keep in mind that they also have a very much weaker interaction with the sphere. Thus, the results are sensitive to the profile in a complex way. Fortunately, Eq. (16) is sufficiently simple that convolution should be straightforward.

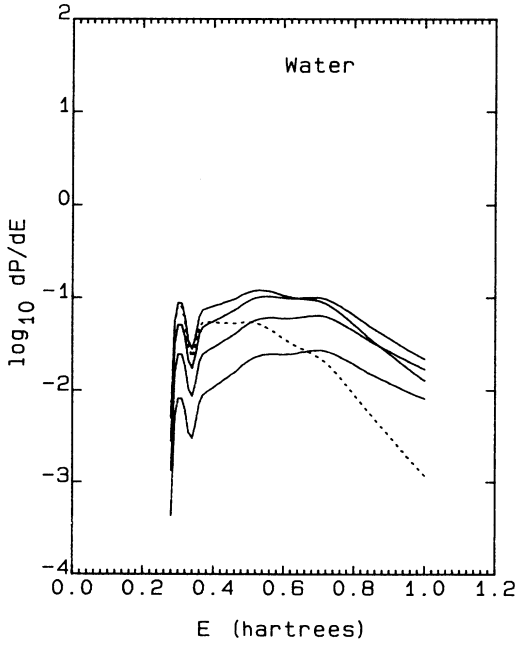

FIG. 6. Same as Fig. 1, except that the sphere is a water droplet.

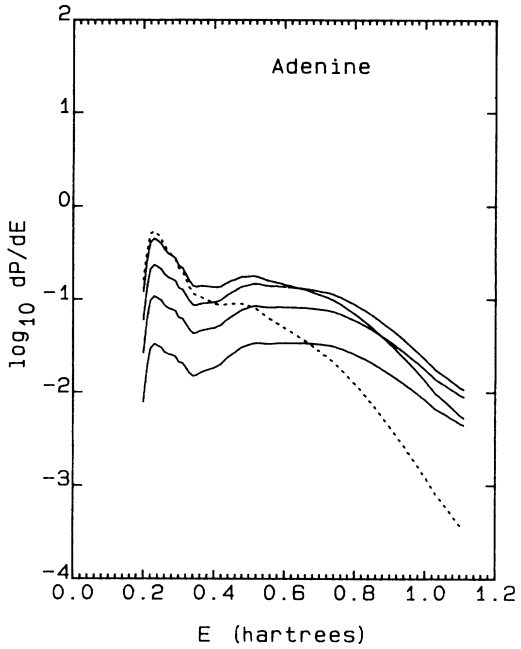

FIG. 7. Same as Fig. 1, except that the sphere is made of adenine.

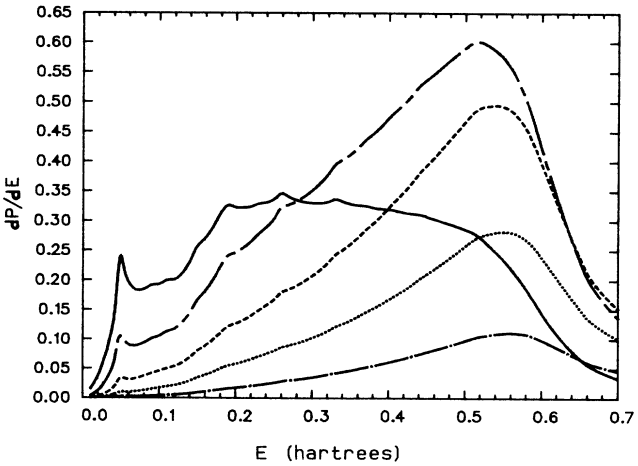

FIG. 8. Differential energy loss probability dP/dE vs the energy loss E in Hartree atomic units for the same impact parameter sphere radius and incident energies as the other figures, but for an aluminum sphere surrounded by manganese. The 100-eV incident beam energy is here shown as a solid curve and other beam energies have descending peak heights with increasing energy.

V. CONCLUSIONS

We have obtained a succinct result for the differential probability of energy loss to a sphere by charged particles in aloof scattering. The results are given for a sphere or spherical void embedded in another medium and for a sphere or spherical void with a layer and with a surrounding medium. The formulas have been applied to electron scattering from spheres of radius 10 nm for several materials. No account of beam profile is given, and the case in which the beam enters the sphere is not considered. Retardation, spatial dispersion, and relativistic effects have been neglected. For spheres of radius 2—20 nm, retardation and spatial dispersion are in fact negligible. The effects of spatial dispersion in scanning transmission electron microscopy have been discussed by Ritchie and Marusak[19] and by Echenique.[20] Relativistic effects must await considerably more complicated analyses, but may be important in scanning transmission electron microscopy at the higher beam energies.

It would be of value to consider the case in which the trajectory intersects the sphere. In this instance the Fourier transform of the potential of the charge in spherical coordinates is broken up into three integrals, one over the time before entering the sphere, one during the time the charge is inside the sphere, and one for subsequent times. The potential inside the sphere has a different expansion in spherical coordinates, and each of the integrations would have to be carried out numerically. However, the procedure is otherwise identical to that presented above for aloof scattering. The case of spheroidal, rather than spherical targets, is currently under investigation. The results will be submitted at a later date for prolate and oblate spheroids.

Our results demonstrate that for spheres for radii greater than simple clusters and of radii no greater than the limit for which retardation becomes significant, it is important to include many higher modes than the dipole modes, especially for close impact parameters and higher energies. Moreover, we have shown that it is not difficult to include the higher modes for a variety of materials and beam energies.

[1]R. J. Warmack, R. S. Becker, V. E. Anderson, R. H. Ritchie, Y. T. Chu, J. Little, and T. L. Ferrell, Phys. Rev. B **29**, 4375 (1984).

[2]P. E. Batson, *Solid State Commun.* **34**, 477 (1980); Ultramicroscopy **9**, 277 (1982); Phys. Rev. Lett. **49**, 936 (1982).

[3]J. M. Cowley, Surf. Sci. **114**, 587 (1982); P. E. Batson, Ultramicroscopy **18**, 125 (1985); L. D. Marks, Solid State Commun. **43**, 727 (1982).

[4]P. M. Echenique, A. Howie, R. H. Milne, and D. J. Wheatley, Proceedings of the Arizona State University Centennial Symposium on High-Resolution Electron Microscopy, 1985 (unpublished); D. I. Wheatley, A. Howie, and D. McMullen, in *Electron Microscopy and Analysis Group—1983,* IOP Conf. Proc. No. 68, edited by P. Doing (Institute of Physics, London, 1984).

[5]T. L. Ferrell and P. M. Echenique, Phys. Rev. Lett. **55**, 1526 (1985).

[6]E. Fujimoto and K. Komaki, J. Phys. Soc. Jpn. **25**, 1679 (1968); N. Kreibig and P. Zacharias, Z. Phys. **231**, 128 (1970); A. A. Lusknikov and A. Simmov, Z. Phys. B **21**, 357 (1975); D. R. Penn and P. Apell, J. Phys. C **16**, 5729 (1983); P. Das and J. L. Gersten, Phys. Rev. B **27**, 5412 (1983).

[7]N. Barberan and J. Bausells, Phys. Rev. B **15**, 6354 (1985).

[8]J. C. Ashley, T. L. Ferrell, and R. H. Ritchie, Phys. Rev. B **14**, 2177 (1976).

[9]J. C. Ashley and T. L. Ferrell, Phys. Rev. B **14**, 3277 (1976).

[10]T. L. Ferrell, P. M. Echenique, and R. H. Ritchie, Solid State Commun. **32**, 419 (1979); A. A. Lucas, Phys. Rev. B **4**, 2939 (1971); G. D. Mahan, Phys. Rev. B **5**, 739 (1972); R. H. Ritchie, Phys. Lett. **38A**, 189 (1972); P. J. Feibelman, Surf. Sci. **27**, 438 (1971).

[11]A. A. Lucas, E. Katheuser, and R. G. Badro, Phys. Rev. B **2**, 2488 (1970); A. A. Lucas and M. Sunjic, Prog. Surf. Sci. **2**, 75 (1972).

[12]M. C. Cole, Phys. Rev. B **2**, 9739 (1969); P. M. Echenique and J. B. Pendry, Phys. Rev. Lett. **37**, 561 (1966); J. Phys. C **9**, 3183 (1976).

[13]W. Ekardt and D. B. Tranthoai, Surf. Sci. **120**, 38 (1982).

[14]J. A. Stratton, *Electromagnetic Theory* (McGraw-Hill, New York, 1941).

[15]I. S. Gradshteyn and C. M. Ryzhik, *Table of Integrals, Series, and Products,* (Academic, New York, 1980), p. 805.

[6]R. Núñez, P. M. Echenique, and R. H. Ritchie, J. Phys. C **13**, 4229 (1980); M. Sunjic and A. A. Lucas, Phys. Rev. B **3**, 719 (1971).

[17]M. Schmeits, J. Phys. C **14**, 1203 (1981).

[18]Optical data for the various cases were taken from H. J. Hageman, W. Gudat, and C. Kunz, Deutsches Electronen-Synchroton (Hamburg) Report No. DESY-Sr-74/7, 1974 (unpublished), except for water which was taken from G. D. Kerr, R. N. Hamm, M. W. Williams, R. D. Birkhoff, and L. R. Painter, Phys. Rev. **5**, 2523 (1972) and L. R. Painter (private communication), adenine which was taken from E. T. Arakawa, L. C. Emerson, S. I. Juan, J. C. Ashley, and M. W. Williams, Photochem. Photobiol. **44**, 349 (1986), and silicon, which was taken from G. E. Jellison, Jr. and F. A. Modine, Oak Ridge National Laboratory Report No. ORNL/TM-8002, 1982 (available from National Technical Information Service, U. S. Dept. of Commerce, 5285 Port Royal Road, Springfield, Virginia 22161, price code A04).

[19]R. H. Ritchie and A. L. Marusak, Surf. Sci. **4**, 234 (1966).

[20]P. M. Echenique, Philos. Mag. B **52**, L9 (1985).